Available online at
www.mdl.mazedan.com

MTESD

www.mazedan.com

www.mazedan.com/mtesd

LIMIT ANALYSIS OF STRIP FOOTING ON LAYERED SOIL AND IT'S NUMERICAL VALIDATION

LITAN DEBNATH

MAZEDAN TRANSACTIONS ON ENGINEERING SYSTEMS DESIGN
e-ISSN: 2582-8061
Article id-MTESD0202002
Vol-2, Issue-2
Received: 28 Feb 2021
Revised: 20-Apr-2021
Accepted: 28-Apr-2021

Citation: Debnath, L., 2021. Limit Analysis of Strip Footing on Layered Soil and Its Numerical Validation. *Mazedan Transactions on Engineering Systems Design*, 2(2), 5-14.

Abstract

In present study, kinematic approach of limit analysis is used to evaluate the seismic bearing capacity of strip footing. The bearing capacity of strip footings over two-layered soil is investigated. A MATLAB program was used for analyzing the bearing capacity values. Effects of various parameters on two layers of soil have been studied in various situations. Bearing capacity charts are presented by varying cohesion, angle of internal friction and unit weight. The charts can utilizable for any combination of $c_1/c_2,\ D_f/B_0,\ \gamma_1/\gamma_2,\ \phi_1/\phi_2$. Numerical analyses were done by using PLAXIS 2D. The bearing capacity is compared with numerical values and it is seen that the results obtained are reliable.

Keywords: Limit analysis, Pseudo-static, Layered soil, $c-\phi$ soil, Velocity hodograph

1. INTRODUCTION

One of the important problems in soil mechanics is the ultimate bearing capacity of soil. The problem of bearing capacity into a perfectly plastic homogeneous half-space has been described has been described for many years. Many researchers like Prandtl (1920); Reissner (1950); Hill (1924); shield (1954); Chen (1970) had investigated the bearing capacity but effective solutions for layered soil does not exist. Attempts at solving the bearing capacity problem for Mohr-coulomb material using the method of characteristics were reported by Michalowski (1983), Mandel and Salencon (1972). The methods for calculating the bearing capacity of multi-layered soil are reported by Bowles (1988).

Using limit equilibrium consideration many researchers investigated like (Reddy and Srinivasan (1967); Meyerhof (1974); Richards et al. (2003); Ghazavi and Eghbali (2008); Ghosh and Debnath (2017)). Considerations of stability in geotechnical structures include a renewed interest in limit analysis. This is due to new applications, such as reinforced soil Michalowski (1998), it is also due to development of numerical techniques in limit analysis, such as presented by Tamura et al. (1984), Sloan (1988) and Sloan and Kleeman (1994). Upper-bound and lower bound solutions can be found for ultimate loads over non-homogeneous soil layers which were used by (Mandel and Salencon (1953); Chen and Davidson (1973); Florkiewicz (1989); Michalowski and Shi (1993); Michalowski and Shi (1995); Michalowski and Shi (2002)). Mosallanezhad and Moayedi (2017) is investigated ultimate bearing capacity of layered soil according to different conventional techniques. While many researchers have been analyzed the ultimate bearing capacity of strip footing resting on layered soil but most of the works are for the calculation of bearing capacity under static loading conditions. Only Debnath and Ghosh (2018), Debnath and Ghosh (2019) has given the solutions of seismic bearing capacity by using limit equilibrium method with pseudo-static approach. Here an attempt is made to introduce limit analysis method for the evaluation of ultimate bearing capacity of shallow strip footing resting on two-layered $c-\phi$ soil. Attempt is also made to consider the coincident effect of unit weight, surcharge and cohesion.

2. ANALYSIS PROCEDURE

The geometry of the present model is shown in Fig.1.

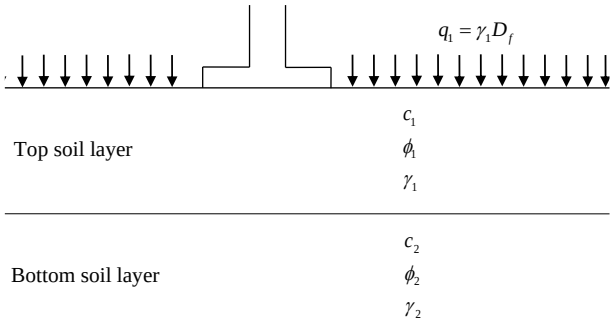

Figure 1 Geometry of footing on two-layered soil profile

Upper bound theorem of analysis

This theorem says, if a compatible mechanism of plastic deformation$\in_{ij}^{p*}$, V_{ij}^{p*} is assumed, which satisfies the condition $V_{ij}^{p*} = 0$ on the displacement boundaryS_v, then the load T_i, F_i determined by equating the rate at which the external forces do work at the rate of internal dissipation of energy will be either higher or equal to the actual limit load, and this can be written as eqn.1

$$\int_v \sigma_{ij}{}^{p*} \in_{ij}{}^{p*} dv \geq \int_s T_i V_i{}^{p*} ds + \int_v F_i V_i{}^{p*} dv \quad (1)$$

The collapse mechanisms were chosen to comprise 2 trapezoidal block ABDE, BDKJ and 2 triangular blocks EDF, DKF as shown in Fig.2. At collapse, the footing and the underlying rigid blocks ABDE, EDF are assumed to move in phase with absolute velocities V_1, V_2 , whereas V_3, V_4 are the absolute velocities of triangular and trapezoidal block EDF and BDKJ. $v_{21}$is the relative velocity of the block EDF with respect to the block of ABDE. V_{32} is the relative velocity of the block EDF with respect to the block DKF. V_{34} is the relative velocity of the block BDKJ with respect to the block FDK. V_{41} is the relative velocity of the block BDKJ with respect to the block ABDE? The interface BD, DF, ED, DK as well as the lines AE, EF, FK and KJ are treated as velocity discontinuity lines. The directions of V_1, V_4, V_2, V_3 makes an angle ϕ_1, ϕ_2 with the corresponding velocity discontinuity lines. Whereas V_{21},V_{34}makes an angle $\phi_2 - \phi_1$ with the discontinuity lines ED and DK. V_{41},V_{32}makes an angle δ_1, δ_2 with discontinuity lines BD, DF. Deformation pattern in present analysis is taken as $\phi_1 < \phi_2$. The present analysis can be also use for deformation pattern$\phi_1 > \phi_2$. It is considered that velocities at weak soil layer are higher than the strong layer. The velocity hodograph is shown in Fig.3.

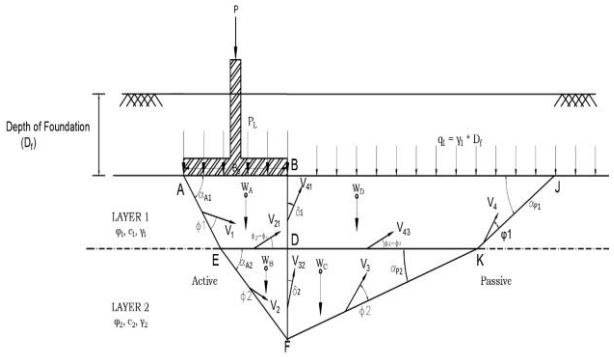

Figure 2 Collapse mechanism of present model

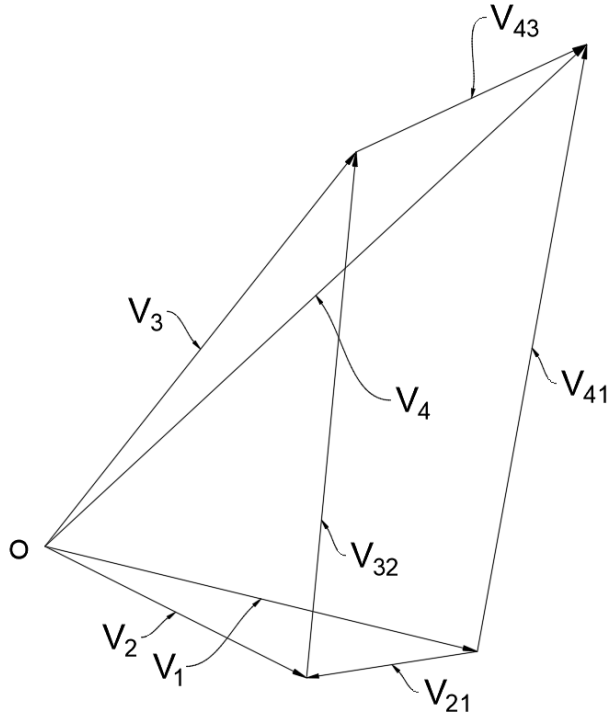

Figure 3 Velocity hodograph of chosen collapse mechanism

External work done

The external work done by different elements can be calculated as follows:

(i) External work done due to the foundation loads are

$$\Delta W_{P_1} = P_L B_0 \left[\sin(\alpha_{A1} - \phi_1)(1 \pm k_v) + \cos(\alpha_{A1} - \phi_1) k_h\right] V_1 \quad (2)$$

$$\begin{aligned} \Delta W_{P_2} &= P_{L_1} ED \left[\sin(\alpha_{A2} - \phi_2)(1 \pm k_v) + \cos(\alpha_{A2} - \phi_2) k_h\right] V_2 \\ &= P_{L_1} (B_0 - h_1 \cot \alpha_{A1}) \left[\sin(\alpha_{A2} - \phi_2)(1 \pm k_v) + \cos(\alpha_{A2} - \phi_2) k_h\right] V_2 \end{aligned} \quad (3)$$

(ii) External work done due to the surcharge loading and the corresponding forces are

$$\begin{aligned} \Delta W_{Q_1} &= Q_1 \left[-\sin(\alpha_{P1} + \phi_1)(1 \pm k_v) + \cos(\alpha_{P1} + \phi_1) k_h\right] V_4 \\ &= \gamma_1 D_f (h_1 \cot \alpha_{P1} + h_2 \cot \alpha_{P2}) \left[-\sin(\alpha_{P1} + \phi_1)(1 \pm k_v) + \cos(\alpha_{P1} + \phi_1) k_h\right] V_4 \end{aligned} \quad (4)$$

$$\begin{aligned} \Delta W_{Q_2} &= Q_2 \left[-\sin(\alpha_{P2} + \phi_2)(1 \pm k_v) + \cos(\alpha_{P2} + \phi_2) k_h\right] V_3 \\ &= \frac{q_1 (h_1 \cot \alpha_{P1} + h_2 \cot \alpha_{P2})^2}{(h_1 + h_1 \cot \alpha_{P1} + h_2 \cot \alpha_{P2})} \left[-\sin(\alpha_{P2} + \phi_2)(1 \pm k_v) + \cos(\alpha_{P2} + \phi_2) k_h\right] V_3 \\ &= \frac{\gamma_1 D_f (h_1 \cot \alpha_{P1} + h_2 \cot \alpha_{P2})^2}{(h_1 + h_1 \cot \alpha_{P1} + h_2 \cot \alpha_{P2})} \left[-\sin(\alpha_{P2} + \phi_2)(1 \pm k_v) + \cos(\alpha_{P2} + \phi_2) k_h\right] V_3 \end{aligned} \quad (5)$$

(iii) External work done due to self-weight and inertia force of trapezoidal zone ABDE is in Eq-6

(iv) External work done due to self-weight and inertia force of triangle EDF is given in Eq-7

(v) External work done due to self-weight and inertia force of trapezoidal zone BJKD is in Eq-8

(vi) External work done due to self-weight and inertia force of triangle DKF is in Eq-9

$$\begin{aligned} \Delta W_A &= W_A \left[\sin(\alpha_{A1} - \phi_1)(1 \pm k_v) + \cos(\alpha_{A1} - \phi_1) k_h\right] V_1 \\ &= \frac{2B_0 - h_1 \cot \alpha_{A1}}{2} h_1 \gamma_1 \left[\sin(\alpha_{A1} - \phi_1)(1 \pm k_v) + \cos(\alpha_{A1} - \phi_1) k_h\right] V_1 \end{aligned} \quad (6)$$

$$\begin{aligned} \Delta W_B &= W_B \left[\sin(\alpha_{A2} - \phi_2)(1 \pm k_v) + \cos(\alpha_{A2} - \phi_2) k_h\right] V_2 \\ &= \frac{B_0 - h_1 \cot \alpha_{A1}}{2} h_2 \gamma_2 \left[\sin(\alpha_{A2} - \phi_2)(1 \pm k_v) + \cos(\alpha_{A2} - \phi_2) k_h\right] V_2 \end{aligned} \quad (7)$$

$$\begin{aligned} \Delta W_C &= W_C \left[-\sin(\alpha_{P1} + \phi_1)(1 \pm k_v) + \cos(\alpha_{P1} + \phi_1) k_h\right] V_4 \\ &= \frac{h_1 \cot \alpha_{P1} + 2h_2 \cot \alpha_{P2}}{2} h_1 \gamma_1 \left[-\sin(\alpha_{P1} + \phi_1)(1 \pm k_v) + \cos(\alpha_{P1} + \phi_1) k_h\right] V_4 \end{aligned} \quad (8)$$

$$\begin{aligned} \Delta W_D &= W_D \left[-\sin(\alpha_{P2} + \phi_2)(1 \pm k_v) + \cos(\alpha_{P2} + \phi_2) k_h\right] V_3 \\ &= \frac{h_2^2 \cot \alpha_{P2}}{2} \gamma_2 \left[-\sin(\alpha_{P2} + \phi_2)(1 \pm k_v) + \cos(\alpha_{P2} + \phi_2) k_h\right] V_3 \end{aligned} \quad (9)$$

$$\sum [\Delta W]_{ext} = \Delta W_{p_1} + \Delta W_{p_2} + \Delta W_{Q_1} + \Delta W_{Q_2} + \Delta W_A + \Delta W_B + \Delta W_C + \Delta W_D \quad (10)$$

The total external work done is the summation of these six contributions; i.e.; equations (2), (3), (4), (5), (6), (7), (8) and (9)

Incremental internal energy dissipation

Civil Engineering Department, G H Raisoni college of Engineering. and Management, Pune, India
*Corresponding author email- litandbnth4@gmail.com

The different elements of the incremental internal energy dissipations can be calculated as follows:

(i) Along *AE*

$$\Delta D_{AE} = c_1 AE \cos\phi_1 V_1 = c_1 h_1 \cos e c\alpha_{A1} \cos\phi_1 V_1 \quad (11)$$

(ii) Along EF

$$\Delta D_{EF} = c_2 EF \cos\phi_2 v_2 = c_2 h_2 \cos e c\alpha_{A2} \cos\phi_2 v_2 \quad (12)$$

(iii) Along FK

$$\Delta D_{FK} = c_2 FK \cos\phi_2 V_3 = c_2 h_2 \cos e c\alpha_{p2} \cos\phi_2 V_3 \quad (13)$$

(iv) Along *KJ*

$$\Delta D_{KJ} = c_1 KJ \cos\phi_1 V_4 = c_1 h_1 \cos e c\alpha_{p1} \cos\phi_1 V_4 \quad (14)$$

(v) Along *DF*

$$\Delta D_{DF} = c_2 DF \cos\delta_2 V_{32} = c_2 h_2 \cos\delta_2 V_{32} \quad (15)$$

(vi) Along *BD*

$$\Delta D_{BD} = c_1 h_1 \cos\delta_1 V_{41} \quad (16)$$

$$\sum[\Delta D] = \Delta D_{AE} + \Delta D_{EF} + \Delta D_{FK} + \Delta D_{KJ} + \Delta D_{DF} + \Delta D_{BD} \quad (17)$$

The total incremental energy dissipation is the summation of these six parts i.e.; equations (11). (12), (13), (14), (15) and (16)

According to the limit analysis principle, the rate of total external work done and the total incremental internal energy dissipation should be become equal. Hence, the bearing capacity can be expressed as eqn.18:

$$p_L = \frac{1}{2}\bar{\gamma} B_0 N_{\gamma''} \quad (18)$$

$N_{\gamma''}$is a single coefficient for coincident effect of cohesion, unit weight and surcharge? In seismic condition $N_{\gamma''}$ is expressed as $N_{\gamma E}$ and static condition as $N_{\gamma S}$

$$N_{\gamma''} = \left(\frac{a_1}{e_1} + \frac{b_1}{e_1} + \frac{2\bar{c}}{\bar{\gamma} B_0}\frac{d_1}{e_1}\right) \quad (19)$$

where, $\bar{c}$ is defined as the weight averaged cohesion.

The detail equations for a_1 ,b_1,d_1 and e_1 are given in "Appendix"

3. RESULTS AND DISCUSSION

Since the heuristic algorithms give us high execution and can be applied in bearing capacity problem hence Particle Swarm Optimization algorithm is applied in the analysis. Fig.4 shows the flowchart of PSO. Results of design chart are represented as graphical reorientation from Fig. 5 to Fig.8. Using these figure seismic bearing capacity factors can be applied in practical field. Fig.5 has shown for ϕ_1=40^0, Whereas, Fig.6, Fig.7 and Fig.8 has shown for ϕ_1=42.5^0, ϕ_1=45^0 and ϕ_1=50^0

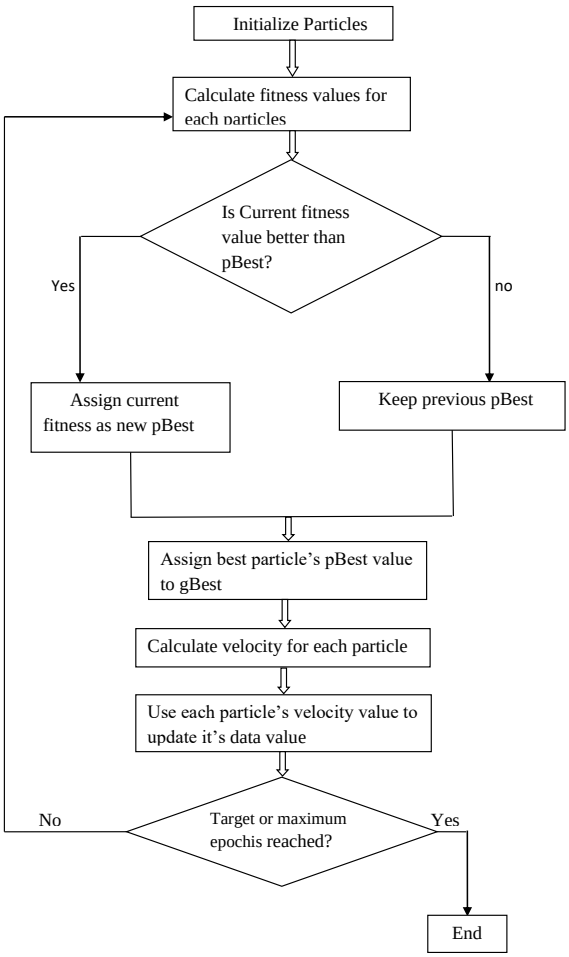

Figure 4 Flowchart of PSO

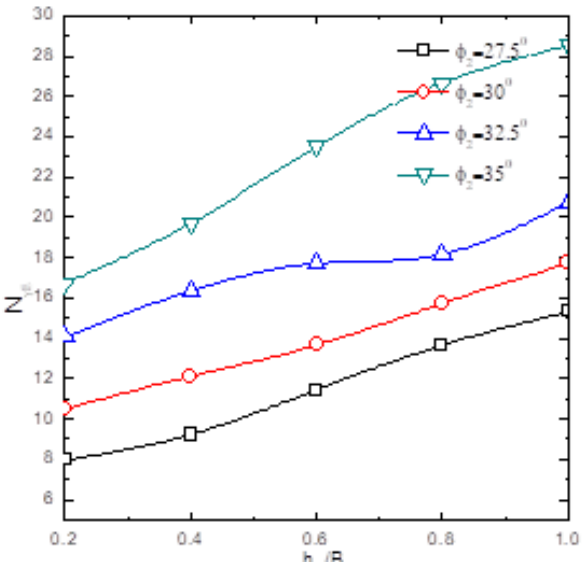

Figure 5 Bearing Capacity factor $N_{\gamma E}$ for ϕ_1=40^0, k_h=0.2, k_v=k_h/2

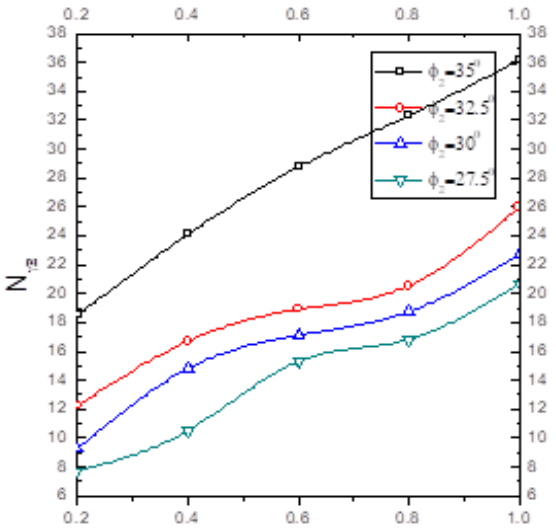

Figure 6 Bearing Capacity factor $N_{\gamma E}$ for $\phi_1=42.2^0$, $k_h=0.2$, $k_v=k_h/2$

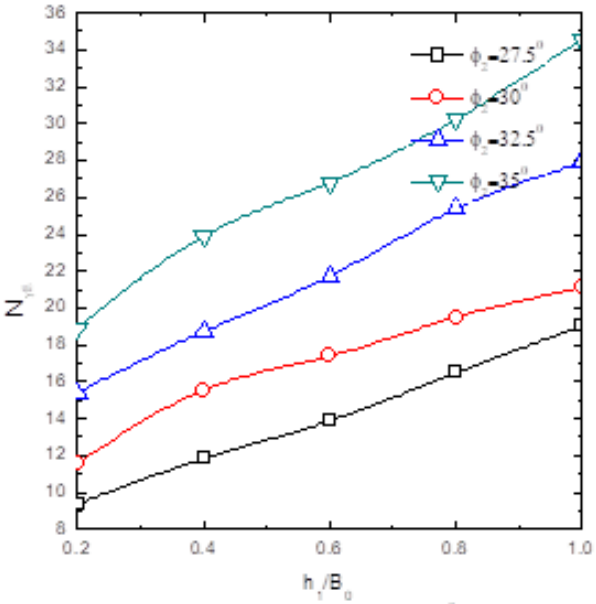

Figure 7 Bearing Capacity factor $N_{\gamma E}$ for $\phi_1=45^0$, $k_h=0.2$, $k_v=k_h/2$

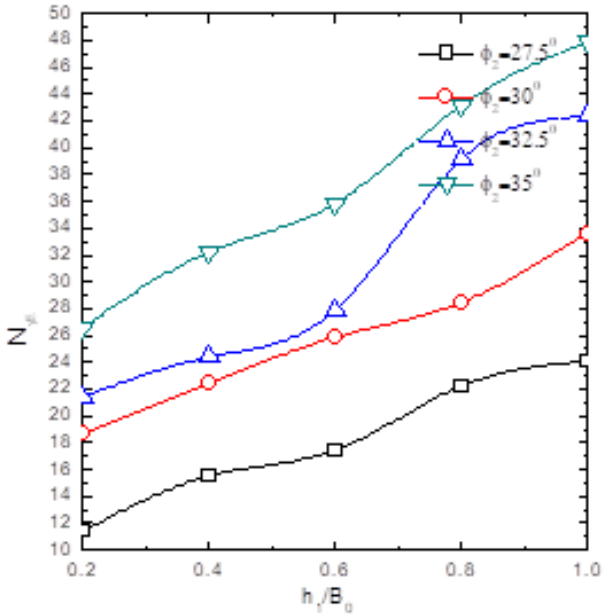

Figure 8 Bearing Capacity factor $N_{\gamma E}$ for $\phi_1=50^0$, $k_h=0.2$, $k_v=k_h/2$

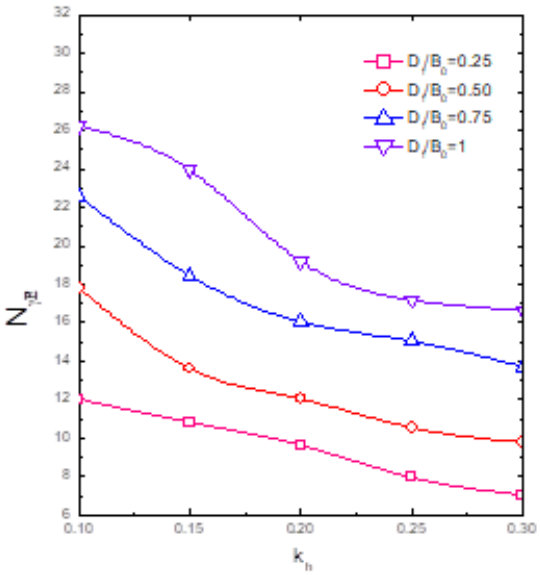

Figure 9 Variation of $N_{\gamma E}$ with k_h for $\phi_2=30^0$, $\delta_2=\phi_1/\phi_2=0.8$, $\delta_2/\delta_2=0.8$, $\phi_2/2$, $k_v=k_h/2$, $k_h=0.2$, $\gamma_1/\gamma_2=0.8$, $h_1/B_0=0.25$, $2c_2/B_0\gamma_2=0.2$, $c_1/c_2=0.8$

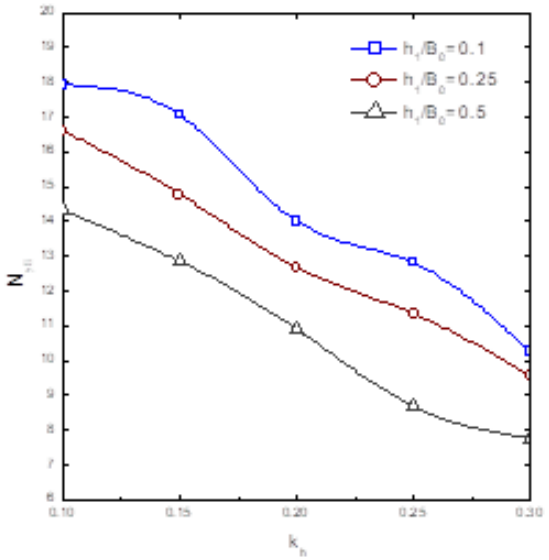

Figure 10 Variation of $N_{\gamma E}$ with k_h for $\phi_2=30^0$, $\delta_2=\phi_1/\phi_2=0.8$, $\delta_1/\delta_2=0.8$, $\phi_2/2$, $k_v=k_h/2$, $k_h=0.2$, $\gamma_1/\gamma_2=0.8$, $D_f/B_0=0.50$, $2c_2/B_0\gamma_2=0.2$, $c_1/c_2=0.8$

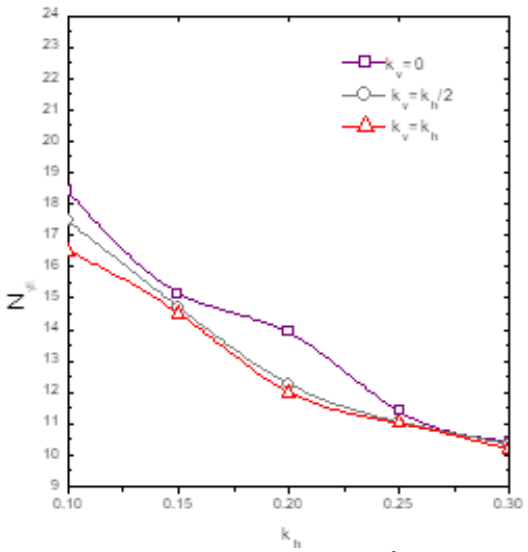

Figure 11 Variation of $N_{\gamma E}$ with k_h for $\phi_2=30^0$, $\delta_2=\phi_2/2$, $\delta_2=\phi_1/\phi_2=0.8$, $\delta_1/\delta_2=0.8$, $\gamma_2=0.2$, $\gamma_1/\gamma_2=0.8$, $D_f/B_0=0.50$, $2c_2/B_0\gamma_2=0.2$, $c_1/c_2=0.8$, $h_1/B_0=0.25$

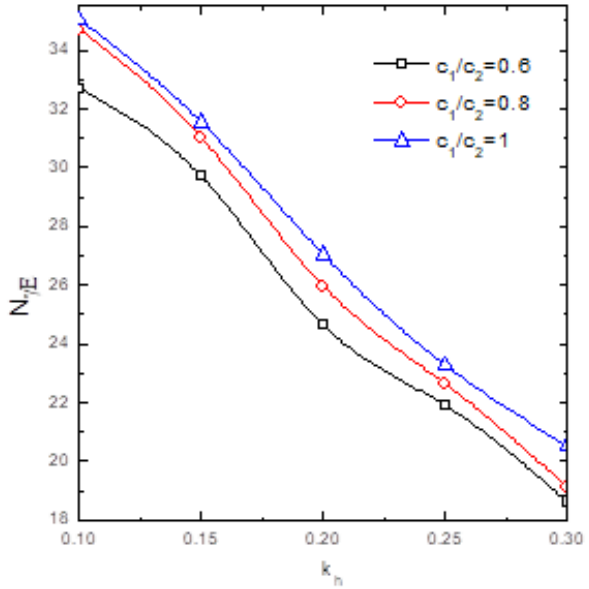

Figure 12 Variation of $N_{\gamma E}$ with k_h for $\phi_2=30^0$, $\delta_2=\phi_2/2$, $\delta_1/\delta_2=0.8$, $k_v=k_h/2$, $\gamma_1/\gamma_2=0.8$, $D_f/B_0=0.50$, $2c_2/B_0\gamma_2=0.2$, $c_1/c_2=0.8$, $h_1/B_0=0.25$

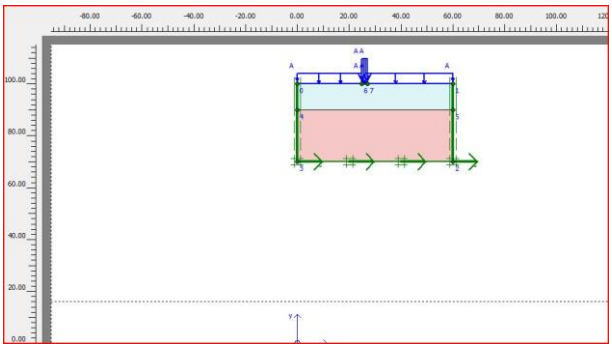

Figure 13 Geometric model of strip footing using PLAXIS software

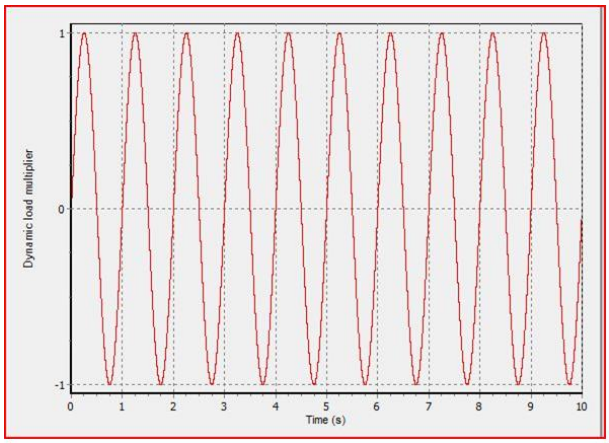

Figure 14 Sinusoidal load of Frequency 1 HZ (base acceleration 0.1g)

4. PARAMETRIC STUDY

The parametric study is done for the variations of pseudo-static seismic bearing capacity coefficients as shown in Figs.9-12.

Variations of seismic bearing capacity coefficients for different values of $\frac{D_f}{B_0}$ using Particle Swarm Optimization Algorithm

Figure 9 depicts the variations of seismic bearing capacity coefficients $(N_{\gamma E})$ at$\phi_2 = 30^0$,$\delta_2 = \frac{\phi_2}{2}$,$\frac{\phi_1}{\phi_2} = 0.8$,$\frac{\delta_1}{\delta_2} = 0.8$, $k_v = \frac{k_h}{2}$,$\frac{\gamma_1}{\gamma_2} = 0.8$,$\frac{h_1}{B_0} = 0.1$,$\frac{2c_2}{\gamma_2 B_0} = 0$,$\frac{c_1}{c_2} = 0$ with k_h . From the plot it is seen that $N_{\gamma E}$ increases with the increase in the value of$\frac{D_f}{B_0}$. It is additionally seen that increase in depth increases the confinement between the soil grains of the sub-structure.

Variations of seismic bearing capacity coefficients for different values of $\frac{h_1}{B_0}$ using Particle Swarm

Optimization Algorithm

Figure 10 shows the variations of seismic bearing capacity coefficients $(N_{\gamma E})$ at$\phi_2 = 30^0$,$\delta_2 = \frac{\phi_2}{2}$,$\frac{\phi_1}{\phi_2} = 0.8$, $\frac{\delta_1}{\delta_2} = 0.8$,$k_v = \frac{k_h}{2}$,$\frac{\gamma_1}{\gamma_2} = 0.8$,$\frac{D_f}{B_0} = 0.5$,$\frac{2c_2}{\gamma_2 B_0} = 0$,$\frac{c_1}{c_2} = 0$ with k_h . From the plot it is seen that, $N_{\gamma E}$ decreases with the increase in the value of $\frac{h_1}{B_0}$. Here, h_1 is the depth of the top layer and it is considered in the analysis that it is weaker than the bottom layer.

Variations of seismic bearing capacity coefficients for different values of k_v using Particle Swarm Optimization Algorithm.

Figure 11 shows the variation of $N_{\gamma E}$at$\phi_2 = 30^0$,$\delta_2 = \frac{\phi_2}{2}$,$\frac{h_1}{B_0} = 0.25$, $\frac{\gamma_1}{\gamma_2} = 0.8$,$\frac{\delta_1}{\delta_2} = 0.8$,$\frac{\phi_1}{\phi_2} = 0.8$,$\frac{D_f}{B_0} = 0.5$,$\frac{2c_2}{\gamma_2 B_0} = 0$,$\frac{c_1}{c_2} = 0$ with k_h . From the plot it is seen that,$N_{\gamma E}$ decreases with the increase in $\boldsymbol{k_v}$.

Variations of seismic bearing capacity coefficients for different values of $\frac{c_1}{c_2}$ using Particle Swarm Optimization Algorithm.

Figure 12 shows the variation of $N_{\gamma E}$ at $\phi_2 = 30^0$,$\delta_2 = \frac{\phi_2}{2}, \frac{h_1}{B_0} = 0.25$, $\frac{\gamma_1}{\gamma_2} = 0.8, k_v = \frac{k_h}{2}, \frac{\phi_1}{\phi_2} = 0.8, \frac{D_f}{B_0} = 0.5, \frac{2c_2}{\gamma_2 B_0} = 0$ with k_h . From the plot, it is seen that the coefficient $N_{\gamma E}$ increases with the increase in the value of $\frac{c_1}{c_2}$. Here, $\frac{c_1}{c_2}$ ratio is increased while keeping c_2 as constant. So, obviously due to the increase in $\frac{c_1}{c_2}$ ratio, the value $N_{\gamma E}$ will increase.

5. NUMERICAL MODELING

Geometry of finite element model of strip footing

Fig.13 shows the geometric model developed in the PLAXIS 2D. The plain strain model is used to simulate the foundation soil. The extension of the soil mass was taken 120m wide and 100m depth. A full fixity boundary along with earthquake boundary condition has been applied for the earthquake condition.

Mesh generation

The model is divided into a number of 15 nodded triangular elements and each node has 3 degree of freedom (a) horizontal direction (b) vertical direction and (c) rotational. Small size meshes are generated by global refinement of cluster to get the reliable results. A uniformly distributed loading system 'A' is representing the load coming from the superstructure and the surcharge load.

Material Properties

Four types of soil are considered in present analysis. Table 1 represents all the soil properties.

Table 1 Input soil properties parameters for Plaxis

	Soil 1	Soil 2	Clay	Deep Sand
unit weight at unsaturated condition(γunsat)(KN/m^3)	11	14	16	17
unit weight at saturated condition(γsat)(KN/m^3)	12	16	18	20
Coefficient of permeability at x direction (Kx)(m/s)	1.02x10^{-6}	2.3x10^{-6}	1.16 x10^{-8}	1.16 x10^{-5}
Coefficient of permeability at Y direction (Ky)(m/s)	1.02x10^{-6}	2.3x10^{-6}	1.16 x10^{-8}	1.16 x10^{-5}
Modulus of elasticity€(KN/m2)	11000	15000	10000	40000
Poisson's ratio(v)	0.33	0.25	0.350	0.300
Cohesion(C)(KN/m^2)	2.45	1.8	5	1
Angle of friction(ϕ)	7.4	11	25	32
Angle of dilatancy(ψ)	0	0	0	2

6. NUMERICAL RESULTS AND DISCUSSION

During calculation stage, three steps are adopted, whereas, in 1st stage initial stress or field stress are generated by k_0 (pressure at rest) procedure. In 2nd step, calculations are carried out for plastic analysis where applied vertical load and weight of soil is activated. Calculation is done for dynamic analysis where earthquake data are incorporated by giving sinusoidal load of frequency 1HZ, 2 HZ and 3 HZ under base acceleration of 0.1g manually (Fig.14). In final step, settlement has been calculated from the deformed mesh.

Numerical Results

The numerical result and discussion to yield the ground surface settlement are described in this section. Fig.15, Fig.16, Fig.17 and Fig.18 shows the deformed mesh and vertical displacement after undergoing stages calculations respectively. Table.2 shows the ground surface settlement obtained from the different types of soil.

Table 2 Numerical Solution (Plaxis 8.6 v)

Soil Sample	Depth Factor (D_f/B_0)	Soil Model 1 HZ, settlement (mm)	Soil Model 2 HZ,settlement (mm)	Soil Model 3 HZ Settlement
Sample 1 (Soil 1/ Soil 2)	0.25	10.84	22.35	33.74
	0.5	14.58	29.94	40.08
	1	23.99	48.56	73.13
Sample 2 (Clay/ Sand)	0.25	5.6	8.5	14.79
	0.5	9.24	14.96	24.68
	1	12.98	21.41	32.55

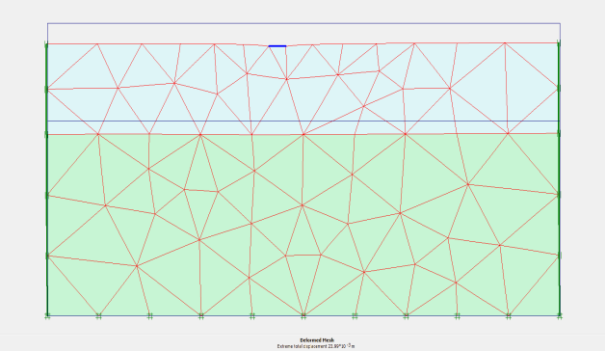

Figure 15 Deformed mesh of soil mass due to applied load

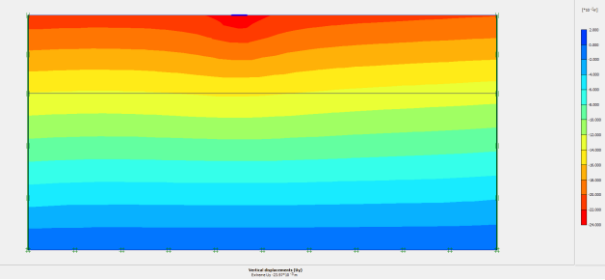

Figure 16 Vertical displacement of soil mass

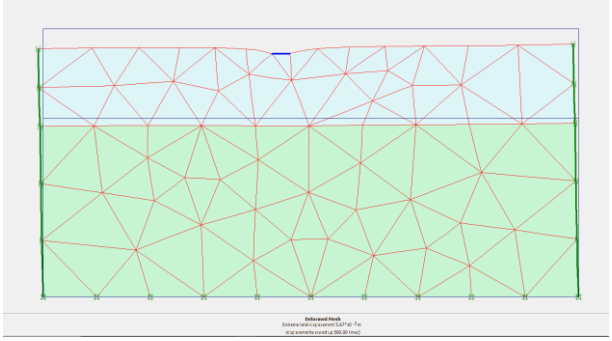

Figure 17 Deformed mesh of soil mass due to applied load

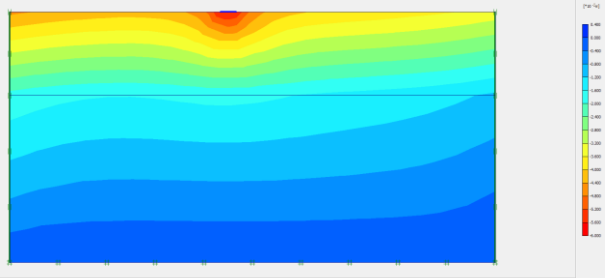

Figure 18 Vertical displacement of soil mass due to vertical seismic load

Numerical validation

Finite element model of shallow strip footing in c-ϕ layered soil is analyzed in Plaxis for the validation of analytical solution. The results obtained from the analytical solution are compared with numerical solution to validate the result. In 1st step settlement of foundation is calculated as follows:

$$S_f = \frac{c_c}{1+e_0} H\, log_{10}\left(\frac{\sigma_0 + \Delta\sigma}{\sigma_0}\right) \quad (20)$$

Where, c_c = compression index; e_0= initial void ratio, H = layer thickness, σ_0= initial pressure, $\Delta\sigma$ = increment of pressure due to superimposed load, $\Delta\sigma = \frac{q_n B_0}{B_0+z}$

Here, q_n= net foundation pressure,

$$q_n = \frac{Q_{ult} - \gamma D_f}{F.O.S} \quad (21)$$

Here, Q_{ult} is the Pseudo-static ultimate bearing capacity which is obtained from analytical solutions.

The earthquake dependent settlement is also calculated by using Richards et al. (1993). Taking the same dynamic soil properties used in numerical modeling in PLAXIS-8.6v is carried out to validate the analytical findings. Results obtained from the analytical solution and numerical modeling has been compared in the Table.3. It is seen that, the settlement obtained from present solutions in on lower side as on increment of D_f/B_0.

$$S_e = 0.174\frac{v^2}{Ag}\left[\frac{k^*_h}{A}\right]^{-4} tan\,\alpha_{AE} \quad (22)$$

Here, v is the peak velocity for the design earthquake (m/sec), A is the acceleration coefficient for the design earthquake, g is the acceleration due to gravity and the value of αAE depends on ϕ and critical acceleration k*.

Comparison with experimental, numerical results

The ultimate bearing capacityq_{ult} has been calculated by using computer programming software 'MATLAB' for various combinations of soil properties in each layer. PSO algorithm is utilized to obtain the optimum bearing capacity coefficient. Table 4 presents the comparison of the average limit pressure with the experimental tests performed by Purushothamaraj et al. (1973), Carlson and Fricano (1961), Koizumi (1965) and Desai and Reese (1970). From this table it has been observed that the present analysis getting virtually more proximate value with other researchers. Table 5-7 shown the Tabular representation of the seismic bearing capacity coefficients for different thickness to footing width ratio(h_1/B_0). From these values, it has been observed that values obtained by present method are higher than Debnath and Ghosh (2018). It is observed that limit analysis method is significantly different (higher value) from Debnath and Ghosh (2018). This optical discernment is due to the reason that Debnath and Ghosh (2018) analyzed the bearing capacity using limit equilibrium method. The advantage of the upper-bound solution over the limit equilibrium solution is that the kinematics are completely verified and the solution is obtained for an associated flow-rule of the material. Table 8 has shown a comparison between the present analyses with Eskavari et al. (2019). From Table 8 it is visually perceived that present analysis getting higher values than Eskavari et al. (2019). The bearing-capacity factors Nc*(qult/c1) for strip, circular, and square footings on two-layered clays are presented in Table 9. As discovered by Merifield et al. (1999), Merifield and Nguyen (2007) all of the analyses herein denote that an intricate relationship subsists between the optically canvassed modes of shear failure and the ratios c1/c2 and h1/B0. The modes of failures can best be described as being either 'general shear', 'partial punching shear', or 'full punching shear' akin to that described by Merifield et al. (1999), Merifield and Nguyen (2007). When comparing the outcomes for square and circular footings to those for strip footings (present evaluation), in standard it became determined that the bearing-capability factors Nc* for square and circular footings had been much extra proximate for strip footings. To demonstrate the potentiality of the present analysis, Finite element (FE) evaluation has been as compared with present values. FE analyses have been performed via Ghazavi and Eghbali (2008) with the aid of utilizing PLAXIS-2D. The physical and mechanical properties of soil every layer is depicted in Table 11, while $\frac{D_f}{B_0}$ratios for different geometries are evinced in Table 10. Table 12 compares the present analysis with the analytical and FEM values obtained by means of Ghazavi and Eghbali (2008). Values obtained by present method are higher than the Finite element analysis. As optically discovered, the outcomes acquired from the present evaluation are extraordinarily well comparable.

Table 3 Comparison of settlement obtained from Analytical and Numerical solution

	Soil Samples			Sample 1			Sample 2	
	(D_f/B_0)		0.25	0.5	1	0.25	0.5	1
Analytical solution using		Saran and Agarwal, 1991	12.19	17.07	25.61	23.17	32.93	47.56
		Richards et al 1993	14.72	9.51	5.37	18.31	13.74	8.94
Numerical solution using		Plaxis-8. ov [H-S Small Model	10.84	14.58	23.99	5.6	9.24	12.98

Table 4 Comparison with Field and Experimental values

Source	Footing type				Bearing pressure(tons/ft2)	
		d/b	c2/c1	ϕ(degrees)	Observed	Present method
Carlson and Fricano (1961)	Circular tank (150ft dia)	0.087	0.18		1.37	5.55
Koizumi (1965)	Circular (2 in. dia.)	0.8	0.33	0.0	6.00b	4.88
Desai and Reese (1970b)	Circular (3 in. dia.)	0.55	1.80	0.0	2.50b	3.85
Purushothamaraj et al. (1973)	Strip footing	0.49	0.50	2.0	0.46	1.22

Table 5 Comparison with analytical values

						Debnath and Ghosh (2018)	Present analysis

						k_h=.0.1			K_h=0.1		
ϕ_2	ϕ_1/ϕ_2	δ_2	δ_1/δ_2	γ_1/γ_2	K_v	h1/B0=0.1			h1/B0=0.1		
						D_f/B_0			D_f/B_0		
						0.25	0.5	1	0.25	0.50	1
					0	14.63	19.94	30.55	14.87	20.73	31.23
30	0.8	15	0.8	0.8	$k_h/2$	14.33	19.82	29.48	14.41	20.02	30.30
					k_h	13.95	19.22	29.18	13.99	19.98	30.28
					0	15.39	21.77	34.22	16.18	22.92	35.02
30	1		1	1	$k_h/2$	15.29	21.70	33.87	16.97	22.54	34.73
					k_h	14.74	21.06	32.93	15.54	22.19	33.98

Table 6 Comparison with Analytical values

						Debnath and Ghosh (2018)			Present analysis		
						k_h=.0.1			K_h=0.1		
ϕ_2	ϕ_1/ϕ_2	δ_2	δ_1/δ_2	γ_1/γ_2	K_v	h1/B0=0.25			h1/B0=0.25		
						D_f/B_0			D_f/B_0		
						0.25	0.5	1	0.25	0.50	1
					0	11.89	16.49	26.79	12.84	17.31	27.88
30	0.8	15	0.8	0.8	$k_h/2$	11.58	15.90	25.97	12.69	16.86	26.54
					k_h	11.02	15.63	24.95	12.24	16.66	25.55
					0	12.29	18.29	28.31	13.68	19.01	29.45
30	1	15	1	1	$k_h/2$	11.98	17.40	28.04	13.47	18.12	28.73
					k_h	11.62	16.52	27.60	13.42	17.82	28.05

Table 7 Comparison with Analytical values

						Debnath and Ghosh (2018)			Present analysis		
						k_h=.0.1			K_h=0.1		
ϕ_2	ϕ_1/ϕ_2	δ_2	δ_1/δ_2	γ_1/γ_2	K_v	h1/B0=0.50			h1/B0=0.50		
						D_f/B_0			D_f/B_0		
						0.25	0.5	1	0.25	0.50	1
					0	9.37	13.95	22.42	9.34	14.15	22.35
30	0.8	15	0.8	0.8	$k_h/2$	9.24	13.60	21.44	9.28	13.88	21.74
					k_h	9.11	13.47	21.08	9.96	13.66	21.14
					0	9.76	14.34	23.70	10.69	16.16	23.81
30	1	15	1	1	$k_h/2$	9.75	14.18	23.26	9.89	15.81	23.99
					k_h	9.56	14.00	22.72	9.72	15.73	22.90

Table 8 Comparison with numerical values

Ultimate Bearing capacity q_u (kPa)									
		Eskavari et al. (2019)				Present Analysis			
$h_1/B0$		ϕ2=27.5, ϕ1=40	ϕ2=30, ϕ1=40	ϕ2=32.5, ϕ1=40	ϕ2=35, ϕ1=40	ϕ2=27.5, ϕ1=40	ϕ2=30, ϕ1=40	ϕ2=32.5, ϕ1=40	ϕ2=35, ϕ1=40
0.6	L.B	360	510	700	970	415.54	541.77	801.377	915.89
	U.B	400	530	720	1050				
0.9	L.B	400	540	730	1020	468.765	554.15	874.41	1073.90
	U.B	440	560	800	1150				
1.2	L.B	470	560	780	1100	536.58	672.70	995.94	1437.72
	U.B	500	620	870	1200				
1.5	L.B	520	600	800	1200	572.814	706.612	1077.117	1623.35
	U.B	540	680	910	1260				

Table 9 Comparison of bearing capacity factor (Nc*) with present analysis

		UB (Merifield et al. 1999)	Merifield and Nguyen (2006) Displacement FEM		Present Study
h_1/B_0	c_1/c_2	Strip Footing	Square Footing	Circular Footing	Strip Footing
0.125	0.2	8.55	7.96	7.95	8.6243
	0.25	8.55	7.96	7.95	8.6243
	0.4	8.55	7.96	7.95	8.6243
	0.5	8.55	7.96	7.89	8.6243
	0.8	6.36	6.73	6.85	6.8934
	1	5.32	5.95	6.05	6.6538
	1.25	4.52	5.11	5.27	5.5429
	1.5	3.93	4.53	4.66	4.9067
	2	3.09	3.73	3.85	4.4638
	2.5	2.61	3.21	3.32	4.337
	4	1.82	2.33	2.41	2.500
	5	1.55	2	2.07	2.4432
0.25	0.2	6.52	6.35	6.36	6.8208
	0.25	6.52	6.35	6.36	6.8208
	0.4	6.52	6.35	6.36	6.8208
	0.5	6.52	6.35	6.36	6.8208
	0.8	6.25	6.27	6.34	6.9867
	1	5.32	5.95	6.05	6.570
	1.25	4.6	5.45	5.59	6.1215
	1.5	4.08	5.03	5.17	5.3611
	2	3.34	4.39	4.51	4.9751

	2.5	2.88	3.92	4.02	4.7776
	4	2.12	3.04	3.13	3.6041
	5	1.85	2.7	2.78	2.8726
0.5	0.2	5.49	5.96	6.04	6.3481
	0.25	5.49	5.96	6.04	6.3481
	0.4	5.49	5.96	6.04	6.3481
	0.5	5.49	5.96	6.04	6.3481
	0.8	5.49	5.96	6.04	6.3481
	1	5.32	5.96	6.05	6.3481
	1.25	4.94	5.94	6.04	6.2816
	1.5	4.48	5.82	6.02	5.9871
	2	3.89	5.46	5.9	5.8864
	2.5	3.47	5.08	5.58	5.2293
	4	2.74	4.22	5.23	4.5314
	5	2.44	3.89	4.39	4.30

Table 10 Various soil and footing, Geometries for comparative studies (Ghazavi and Eghbali, 2008)

B_0 Footing Width (m)	q Overburden Pressure (KN/m^2)	h_1/B_0
1	10	For all three cases h_1/B_0 varies from 0.1 up to 1
2	17.5	
3	25	

Table 11 Properties of soil of each layer used in comparative studies (Ghazavi and Eghbali, 2008)

Case	Friction angle φ	Unit weight γ (KN/m^3)	Elasticity modulus E (KN/m^2)	Poisson's ratio ν
1	30	19	17,500	0.333
2	31	19.3	20,000	0.327
3	33	19.9	25,000	0.313
4	34	20.1	27,500	0.306
5	36	20.5	35,000	0.291
6	37	20.7	40,000	0.285
7	39	20.9	50,000	0.27
8	42	21.1	65,000	0.249

Table 12 Comparisons of bearing capacity results obtained from present analysis with other authors and PLAXIS analysis

B_0=1m	No	h_1/B_0	Ghazavi and Eghbali (2008)	**Plaxis** Ghazavi and Eghbali (2008)	Present
	1	0.25	475	572	538.07
	2	0.5	450	498	500.11
	3	0.75	424	456	480.10
	4	1	396	385	469.78
	5	1.25	368	382	457.4
B_0=2m	1	0.25	904	992	1040.74
	2	0.5	856	860	940.05
	3	0.75	806	835	835.47
	4	1	754	776	819.37
	5	1.25	699	766	779.56
B_0=3m	1	0.25	1333	1403	1599.0
	2	0.5	1263	1210	1108.9
	3	0.75	1189	1263	1083.34
	4	1	1111	991	1064.03
	5	1.25	1029	969	946.34

7. CONCLUSIONS

In present study upper bound solution is presented for the calculation of bearing capacity of a two-layered c-ϕ soil. The simplicity of the solution to the relatively perplexed quandary of the bearing capacity of footings over two different soils was achieved by introducing a failure mechanism where the velocity discontinuities were bent at specific angles at the interface of layers. This allowed one to construct a simple hodograph. The solution is predicted on the classical approach in which the geometry of hodograph is modified in search of the least upper bound. Optimization of the geometry of the mechanism led to the least upper bound. This approach seems to be very effective, and it yields better results than Debnath and Ghosh (2018). An attempt has also made to evaluate the seismic bearing capacity for simultaneous resistance of unit weight, surcharge and cohesion. On the basis of analysis, it is seen that seismic bearing capacity values decreases if the values of horizontal and vertical seismic acceleration coefficients are increased. Validation of numerical results with the analytical solution gives the good agreement. It is seen from the comparative study; the present analysis gives closer value with other researcher's value. The bearing capacity factor $N_{\gamma''}$ for the case of two layered soil with constant friction angle has been presented in the form of design charts which can be usable in practical field.

CONFLICT OF INTEREST

There is no conflict of interest in the analysis

DATA AVAILABILITY STATEMENT

The authors confirm that some data and code generated during this study are proprietary or confidential in nature and may only be provided with restrictions e. g.

(a) MATLAB Code

(b) Particle Swarm optimization code

(c) Limit Analysis hodograph

(d) Conversion of Relative velocity

(e) Graphical representation of all parameters

REFERENCES

[1] Bowles (1988) Foundation analysis and design. 4th Ed. McGraw Hill, New York, N.Y.

[2] Button (1953) The bearing capacity of footings on a two-layer cohesive subsoil. Proceedings, 3rd International Conference on soil Mechanics and Foundation Engineering, 111: 712-729

[3] Carlson, E. D., and Fricano, S. P. (1961) Tank foundation in eastern Venezuela. J. Soil Mech. Found. Div. ASCE, 87, 69-90.

[4] Chen and Davidson, H. l. (1973) Bearing capacity determination by limit analysis, J. soil Mech. Found. Div. 99(6), 433-449

[5] Chen, W. F., (1970) Limit Analysis and Soil Plasticity, Elsevier-Scientific Publishing Co., Amsterdam, The Netherlands.

[6] Debnath and Ghosh (2018) Pseudo-static analysis of shallow strip Footing resting on Two-Layered Soil. Int. J. Geomech., DOI: 10.1061/(ASCE)GM.1943-5622.0001049. Div., 107(7), 915–927.

[7] Debnath and Ghosh (2019) Pseudo-static bearing capacity analysis of Shallow strip footing over two-layered soil considering punching shear failure. Geotech. and Geol. Engg., DOI: 10.1007/s10706-019-00866-5.

[8] Desai, C. S., and Reese, L. (1970) Ultimate capacity of circular footing on Layered soils. J. Indian Nat. Soc. Soil Mech. Found. Eng. 96(1), 41-50.

[9] Eshkevari, S. S., Abbo, J. A. and Kouretzis, G. (2019) Bearing capacity of strip footings on Layered sands. Computers and Geotechnics., DOI: 10.1016/j.compgeo.2019.103101.

[10] Florkiewicz. A. (1989) Upper bound to bearing capacity of layered soils. Can. Geotech. J. 26(4). 730-736

[11] Ghazavi and Eghbali (2008) A simle limit equilibrium approach for calculation of ultimate bearing capacity of shallow foundations on two-layered granular soils. Geotech. Geol.Eng., 26(5),535-542

[12] Ghosh and Debnath (2017) Seismic bearing capacity of shallow strip footing with coloumb failure mechanism using limit equilibrium method. Geotech. and Geol. Engg., DOI: 10.1007/s10706-017-0268-y.

[13] Hill (1950) The mathematical theory of plasticity Clarendon press, Oxford, United Kingdom.

[14] Koizumi, Y. (1965). Discussion on session 4-Division 3. Proc. Sixth Int. Conf. Soil Mech. Found. Engg., Montreal, Que. 3. pp. 413-415.

[15] Mandel and Salencon (1972) Force portante d'un sol surune assise rigide 9etude theoretique. Geotechnique, 22: 79-93

[16] Merifield, R.S., and Nguyen, Q. V. (2007) Two- and three-dimensional bearing-capacity solutions for footings on two layered clays. Geomech. and GeoEngg.,1(2),151-162.

[17] Merifield, R.S., and Sloan, S.W. (1999) Rigorous plasticity solutions forthebearing capacity of two-layered clays. Geotechnique,49(4),471-490.

[18] Meyerhof, G. G. (1974) Ultimate Bearing Capacity ofFootings on Sand Layer Overlying Clay, Canadian Geotechnical Journal, DOI: 10.1139/t74-018, 11(2),223-229.

[19] Michalowski (1983) On the solution of plane flow of granular media for jump non-homogeneity. International journal for Numerical and Analytical methods in Geomechanics,7:485-492

[20] Michalowski and Shi. (1993) Bearing capacity of non-homogeneous clay layers under embankments. J. Geotech. Engrg.ASCE.119(10), 1657-1669

[21] Michalowski, R. L, Shi, L. (1995) Bearing Capacity of Footings over two layers foundation soils. J. Geotech. Engg. Vol. 5, No.421, pp.421-428.

[22] Michalowski, R. L. (1998) Limit analysis in stability calculations of reinforced soil structures. Geotextiles and Geomembranes 16(6): 311–331.

[23] Michalowski, R. L. (2002) Collapse loads over two-layer clay foundation soils. Soils and Foundation, vol. 42, No.1, pp.1-7.

[24] Mosallanezhad, Mand Moayedi, H (2017) Comparison Analysis of Bearing Capacity Approaches for the Strip Footing on Layered Soils.Arab J SciEng.42(9),3711–3722.

[25] overlying soft Clay." Can.Geotech.J..17(2).300-303

[26] Prandtl (1920) Uber die Harte plastischer korper. Nachr. Ges.wissensch, Gottiingen, math-phys. Klasse. 74-85 (in German)

[27] Purushothamaraj, P., Ramiah, K. B. and Venkatakrishna, N. K (1973) Bearing Capacity of Strip Footings in Two Layered Cohesive-friction Soils. Can. Geotech. J. Vol.11, pp. 32-45.

[28] Reddy and Srinivasan (1967) Bearing capacity of footings on layered clays. J. soil. Mech. Found. Div. ASCE. 93(2). 83-99

[29] Reissner (1924) Zum Erddruckproblem. "Proc, First Int. Congr for Appl. Mech. C.B. Biezeno and J.M.Burgers.Eds. Technische Boekhandel en Drukkerii J. Waltman Jr. The Netherlands, Delft .295-311

[30] Richards, R, Elms, D, G, and Budhu, M, (1993) Seismic Bearing Capacity and Settlements of Foundations, J. Geotech. Eng., ASCE, vol-119(4), pp-662-674.

[31] Rychlewski (1966) Plain plastic strain for jump non-homogeneity. Int. J. Nonlinear mechanics, 1(1): 57-78

[32] Saran, S, and Agarwal, R, K, (1991) Bearing Capacity of Eccentrically Obliquely Loaded Footing, J. Soil Mech. Found. Div., ASCE, vol-117(11), pp-1669-1690.

[33] Shield (1954) Plastic potential theory and Prandtl bearing capacity solution. J. Appl. Mech., 21(2), 193-194

[34] Sloan, S. W. (1988) Lower bound limit analysis using finite elements and linear programming. Int. J. Num. Analyt. Mech. Geomech., 12, 61-67.

[35] Sloan, S. W. and Kleeman, P. W. (1994) Upper bound limit analysis using discontinuous velocity fields, Res. Report No. 096.05.1994, University of Newcastle, Australlia.

[36] Tamura, T., Kobayashi, S. and Sumi, 'I. (1984) Limit analysis of soil structure by rigid plastic finite element method, Soils and Foundations, 24 (1), 34-42.

APPENDIX

$$a_1 = \left(2 - \frac{h_1}{B_0}\cot\alpha_{A1}\right)\frac{h_1}{B_0}\frac{\gamma_1}{\bar{\gamma}}\left[\sin\left(\alpha_{A1} - \phi_1\right)\left(1 \pm k_v\right) + \cos\left(\alpha_{A1} - \phi_1\right)k_h\right] V_1$$

$$+ \left(1 - \frac{h_1}{B_0}\cot\alpha_{A1}\right)\frac{h_2}{B_0}\frac{\gamma_2}{\bar{\gamma}}\left[\sin\left(\alpha_{A2} - \phi_2\right)\left(1 \pm k_v\right) + \cos\left(\alpha_{A2} - \phi_2\right)k_h\right] V_2$$

$$+ \left(\frac{h_1}{B_0}\cot\alpha_{P1} + 2\frac{h_2}{B_0}\cot\alpha_{P2}\right)\frac{h_1}{B_0}\frac{\gamma_1}{\bar{\gamma}}\left[-\sin\left(\alpha_{P1} + \phi_1\right)\left(1 \pm k_v\right) + \cos\left(\alpha_{P1} + \varphi_1\right)k_h\right] V_4$$

$$+ \frac{h_2^2\cot\alpha_{P2}}{B_0}\frac{\gamma_2}{\bar{\gamma}}\left[-\sin\left(\alpha_{P2} + \varphi_2\right)\left(1 \pm k_v\right) + \cos\left(\alpha_{P2} + \phi_2\right)k_h\right] V_3$$

$$b_1 = 2\left(\frac{\gamma_1}{\bar{\gamma}}\right)\left(\frac{D_f}{B_0}\right)\left(\frac{h_1}{B_0}\cot\alpha_{P1}+\frac{h_2}{B_0}\cot\alpha_{P2}\right)\left[-\sin\left(\alpha_{P1}+\phi_1\right)\left(1\pm k_v\right)+\cos\left(\alpha_{P1}+\phi_1\right)k_h\right]V_4$$

$$+2\frac{\left(\frac{\gamma_1}{\bar{\gamma}}\right)\left(\frac{D_f}{B_0}\right)\left(\frac{h_1}{B_0}\cot\alpha_{P1}+\frac{h_2}{B_0}\cot\alpha_{P2}\right)^2}{\left(\frac{h_1}{B_0}+\frac{h_1}{B_0}\cot\alpha_{P1}+\frac{h_2}{B_0}\cot\alpha_{P2}\right)}\left[-\sin\left(\alpha_{P2}+\phi_2\right)\left(1\pm k_v\right)+\cos\left(\alpha_{P2}+\phi_2\right)k_h\right]V_3$$

$$d_1 = \left[\begin{array}{l}\left(\frac{c_1}{\bar{c}}\right)\left(\frac{h_1}{B_0}\right)\cos ec\,\alpha_{A1}\cos\phi_1+\left(\frac{c_2}{\bar{c}}\right)\left(\frac{h_2}{B_0}\right)\times\cos ec\,\alpha_{A2}\cos\phi_2\,V_2\\ +\left(\frac{c_2}{\bar{c}}\right)\left(\frac{h_2}{B_0}\right)\cos ec\,\alpha_{P2}\cos\phi_2\,V_3+\left(\frac{c_1}{\bar{c}}\right)\left(\frac{h_1}{B_0}\right)\cos ec\,\alpha_{P1}\cos\phi_1\,V_4\\ +\left(\frac{c_2}{\bar{c}}\right)\left(\frac{h_2}{B_0}\right)\cos\delta_2\,V_{32}+\left(\frac{c_1}{\bar{c}}\right)\left(\frac{h_1}{B_0}\right)\cos\delta_1\,V_{14}\end{array}\right]$$

$$e_1 = \left[\sin\left(\alpha_{A1}-\phi_1\right)\left(1\pm k_v\right)+\cos\left(\alpha_{A1}-\phi_1\right)k_h\right]v_1$$

$$+\frac{1}{1+\frac{h_1}{B_0}}\left(1-\frac{h_1}{B_0}\cot\alpha_{A1}\right)\left[\sin\left(\alpha_{A2}-\phi_2\right)\left(1\pm k_v\right)+\cos\left(\alpha_{A2}-\phi_2\right)k_h\right]v_2$$